DYNAMIC ANALYSIS OF MOISTURE TRANSPORT THROUGH WALLS AND ASSOCIATED COOLING LOADS IN THE HOT/HUMID CLIMATE OF FLORIANÓPOLIS, BRAZIL

N. Mendes[1] and F. C. Winkelmann
Energy and Environment Division
Lawrence Berkeley National Laboratory
Berkeley, CA 94720, USA

R. Lamberts, P.C. Philippi and J.A.B. Da Cunha Neto
Federal University of Santa Catarina
Mechanical Engineering Department
Florianópolis - SC 88049-900, Brazil

ABSTRACT
We describe the use of a dynamic model of combined heat and mass transfer to analyze the effects on cooling loads of transient moisture storage and transport through walls with porous building materials, under varying boundary conditions.

The materials studied were brick, lime mortar and autoclaved cellular concrete. The physical properties of these materials, such as mass transport coefficients, thermal conductivity and specific heat, were taken to be functions of moisture content.

moisture effects. Also analysed were the influence on cooling loads of high moisture content due to rain soaking of materials, and the influence of solar radiation on sunny and cloudy days. The weather used was a hot/humid summer period in Florianópolis (South Brazil).

It is shown that neglecting moisture migration or assuming that the physical properties of wall materials do not depend on moisture content can result in large errors in sensible and latent heat transfer.

1. INTRODUCTION

In building energy analysis, calculated heat conduction through walls usually neglects the storage and transport of moisture in the porous structure of the walls. However, walls are normally subject to both thermal and moisture gradients so that an accurate heat transfer determination requires a simultaneous calculation of both sensible and latent effects. The transfer of moisture through common building materials, such as wood, concrete and brick, depends on the complex morpho-topological characteristics of the pores in these materials.

Besides its effect on heat transfer, moisture has other implications, especially in hot/humid climates. It is mold and mildew, affecting the health of building occupants.

Several investigators have developed models for moisture transport in buildings. Cunningham (1988) developed a mathematical model for hygroscopic materials in flat structures that uses an electrical analogy with resistances for the vapor flow and an exponential approximation function with constant mass transport coefficients. Keresteciogiu and Gu (1989) investigated the phenomenon using evaporation-condensation theory in the pendular state (unsaturated liquid flow stage). The application of this theory is limited to low moisture content. Burch and Thomas (1991) developed a computational model, MOIST, using the finite-difference method to estimate the heat and mass transfer through composite walls under non-

[1] Visiting Ph.D. Student from Federal University of Santa Catarina, Florianópolis, Brazil.

isothermal conditions. The thermal conductivity was considered constant and the latent heat due to phase change within the wall was neglected. This program is also limited to low moisture content. El Diasty et al. (1993) used an analytical approach that assumed isothermal conditions and constant transport coefficients. Liesen (1994) used evaporation-condensation theory and a response factor method to develop and implement a model of heat and mass transfer in the building thermal simulation program IBLAST (Integrated Building Loads Analysis and System Thermodynamics). To use this method, hygrothermal property variations were neglected. There is no liquid transfer. This program is restricted to very low moisture content but has the advantage of short calculation time. Yik et al. (1995) developed a simplified model integrated with air-conditioning system component models that employs evaporation-condensation theory with differential permeability. It is a fast model, but only applicable to materials that stay in the pendular state.

We have implemented a new, dynamic model that avoids the assumptions and restrictions of the above approaches. This model allows the cooling loads due to combined heat and moisture transport through walls to be calculated for a wide range of materials, even under extreme conditions in hot/humid climates.

For the walls we consider sensible and latent surface convection, absorbed solar radiation, heat and mass transfer through the wall, and vapor/liquid phase change. The walls are described mathematically using the model of Philip and DeVries (1957) in which vapor and liquid flow under moisture content and thermal gradients. In this model, heat, vapor and liquid flow are taken to be simultaneous and coupled. Physical quantities, such as mass transport coefficients, thermal conductivity and specific heat, are variable and depend on wall temperature and moisture content.

This work analyzes the time dependence of cooling loads and of the thermal and moisture content for three different types of wall material: autoclaved cellular concrete, brick, and lime mortar. The analysis is done at the most critical summer week in the hot/humid climate of Florianopólis, Brazil. Also analyzed is the influence on cooling loads and wall moisture levels for two types of rain conditions: rain followed by a clear week and rain followed by a cloudy week.

2. MATHEMATICAL MODEL

The governing partial differential equations are given by equations (1) and (2). They were derived from conservation of mass and energy flow in an elemental volume of porous material.

Mass conservation equation

$$\frac{\partial \theta}{\partial t} = -\frac{\partial}{\partial x}\left(\frac{j_l}{\rho_l} + \frac{j_v}{\rho_l}\right) \qquad (1)$$

Energy conservation equation

$$\rho_m c_m \frac{\partial T}{\partial t} = \frac{\partial}{\partial x}(\lambda \frac{\partial T}{\partial x}) - L\frac{\partial}{\partial x}(j_v) \qquad (2)$$

Note that equation (2) differs from Fourier's equation by an added convective transport term due to moisture diffusion associated with evaporation and condensation of water in the pores of the medium. The driving forces for convective transport are temperature and moisture gradients.

The parameter c_m is the specific heat, which is a function of θ. The quantity λ is the thermal conductivity of the medium in the absence of phase change. It usually depends strongly on θ and weakly on T.

The vapor and liquid flows are expressed in terms of transport coefficients, D, associated with the thermal and moisture gradients. According to Philip and DeVries (1957), the equations are:

For liquid conservation

$$\frac{j_l}{\rho_l} = -D_{T l}\frac{\partial T}{\partial x} - D_{\theta l}\frac{\partial \theta}{\partial x} \qquad (3)$$

For vapor conservation

$$\frac{j_v}{\rho_l} = -D_{Tv}\frac{\partial T}{\partial x} - D_{\theta v}\frac{\partial \theta}{\partial x} \qquad (4)$$

Boundary Conditions

The outside surface of the wall is exposed to solar radiation, heat and mass convection, and phase change. The associated conservation equations are as follows.

Mass Conservation

Mass convection at the outside surface (x=0)

$$-\frac{\partial}{\partial x}(D_\theta \frac{\partial \theta}{\partial x} + D_T \frac{\partial T}{\partial x})_{x=0} = \frac{h_{m,ext}}{\rho_l}(\rho_{v,ext} - \rho_{x=0}) \qquad (5)$$

Mass convection at the inside surface (x=*l*)

$$\frac{\partial}{\partial x}(D_\theta \frac{\partial \theta}{\partial x} + D_T \frac{\partial T}{\partial x})_{x=l} = \frac{h_{m,int}}{\rho_l}(\rho_{v,int} - \rho_{x=l}) \qquad (6)$$

where:

$D_\theta = D_{\theta l} + D_{\theta v}$;
$D_T = D_{Tl} + D_{Tv}$.

Energy Conservation

Outside surface (x=0)

$$-\left(\lambda \frac{\partial T}{\partial x}\right)_{x=0} - (Lj_v)_{x=0} = h_{ext}(T_{ext} - T_{x=0}) + \alpha q_r + Lh_{m,ext}(\rho_{v,ext} - \rho_{v,x=0}) \qquad (7)$$

where:

$h_{ext}(T_{ext} - T(0))$ = heat convection;
$\alpha\, q_r$ = absorbed solar radiation;
$h_{m,ext}(\rho_{v,ext} - \rho_{v,x=0})$ = phase change energy.

Inside surface (x=*l*)

$$\left(\lambda \frac{\partial T}{\partial x}\right)_{x=l} + (Lj_v)_{x=l} = h_{int}(T_{int} - T_{x=l}) + Lh_{m,int}(\rho_{v,int} - \rho_{v,x=l}) \qquad (8)$$

where:

$h_{int}(T_{x=l} - T_{int})$ = heat convection;
$Lh_{m,int}(\rho_{v,int} - \rho_{v,x=l})$ = phase change energy.

3. SIMULATION PROCEDURE

The above equations were solved with a finite-volume approach using a fully implicit solution scheme with coupling between the conservation equations. Using the Patankar (1980) method with uniform nodal spacing and a tridiagonal-matrix solution algorithm, a C program solves the temperature and moisture content distributions iteratively at each time step.

For accuracy, a 30-second time step was used to simulate a 3.94 in (10 cm) thickness wall. The initial conditions were assumed to be the average between outside and inside temperature and relative humidity. The program was run for 45 days before the week of analysis, almost totally reducing the effect of the assumed the initial conditions. The run time for a 50-node wall on a 66-MHz 486 computer was about three hours to simulate a 52-day period.

The hourly outside air temperature and humidity (Figure 1) were taken from the Test Reference Year weather data for Florianópolis, Brazil. The inside room air was assumed to be conditioned to a comfort condition of 73.4 °F (23 °C) and 60% relative humidity during work hours. When the air conditioning is turned off at 5 pm we have assumed that the inside conditions reach the outside conditions linearly in five hours. When the air conditioning is turned back on at 8 am we assume two hours to reach the comfort condition.

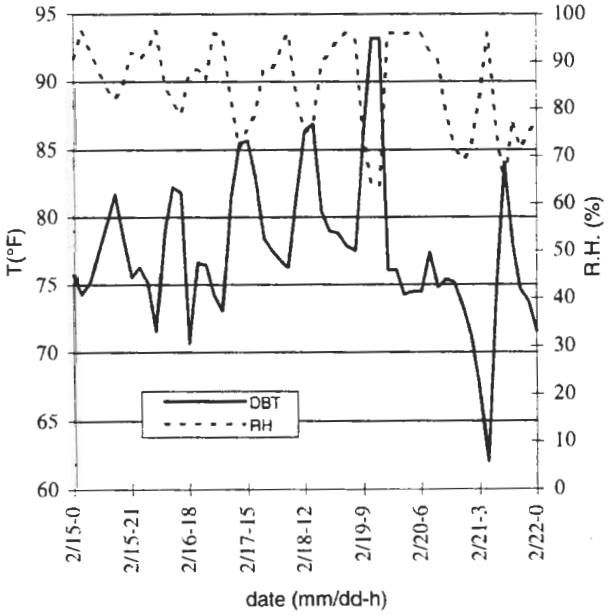

Figure 1: Florianópolis weather for the February 15 to February 22 analysis period.

The input material properties for autoclaved cellular concrete (ACC) were obtained from Da Cunha Neto (1992). Properties for brick (BRK) and lime mortar (LMT) were obtained from Perrin (1985). The available materials' data allows all of the transport coefficients to be modeled as a function of moisture content. The basic material properties used in the simulation are given in Table 1. In this table "open porosity" is the ratio of the volume of open pores (i.e., pores with openings that have a path to both wall surfaces) to the total volume.

Table 1: Basic material properties used in the dry case.

Property	ACC	BRK	LMT
Density [lbm/ft^3]	24.04	118.62	127.98
Open porosity	0.25	0.29	0.18
Thermal conductivity [Btu/hr-ft-°F].	0.049	0.64	1.13
Specific heat [Btu/lbm-°F]	0.2399	0.2198	0.2265

In the simulations the walls are assumed to be composed of a single material, with no surface paint or other moisture barrier.

According to Bogle et al. (1984), depending on the intensity of rainfall, a mean moisture content of up to 20% by volume has been recorded for brick walls. We assumed this level of moisture content, representing the rain effect, to be present in the BRK as well as ACC and LMT walls in the week preceding the analysis week. Actually, the rain simulation that we have done represents a semi-natural drying process after a strong rain fall, since the room air conditioning creates a forced mass flux on the inside surface during work hours.

4. RESULTS

In the following we designate simulation *with moisture in the wall* as "moist," simulation with *rain absorbed by the wall* as "rainy," and simulation *with no moisture in the wall* as "dry." The simulations with and without exterior solar radiation are indicated by "sunny" and "cloudy," respectively. Only one vertical wall is simulated. For the sunny condition the wall is assumed to face south, so that, in Florianópolis (which is south of the equator at latitude -27.5°) it receives little direct radiation.

Dependence On Wall Material

Figure 2 shows simulated moisture profiles (with "moist" simulation) for the three different wall materials at 6am and 6pm on February 20. Here, node 1 is on the outside of the wall and node 50 is on the inside of the wall. We see significant moisture variation with time and distance to a depth of about 0.6 in (1.5cm) at the outside and inside wall surfaces but little variation in the interior of the wall. Other analysis (not shown) indicates that is less true when it rains strongly since then the moisture gradient is much higher and therefore there is more mass diffusion through the wall. The high moisture content at node 50 in the early morning implies a high latent heat transfer when the air conditioner is turned on. The LMT wall shows the highest mean moisture content whereas in the early morning the ACC wall shows the highest peak moisture content. In contrast, the BRK wall shows almost no variation in depth or time because brick has a peculiar structure with a higher number of large pores than the other materials, which inhibits moisture fixation by capillarity.

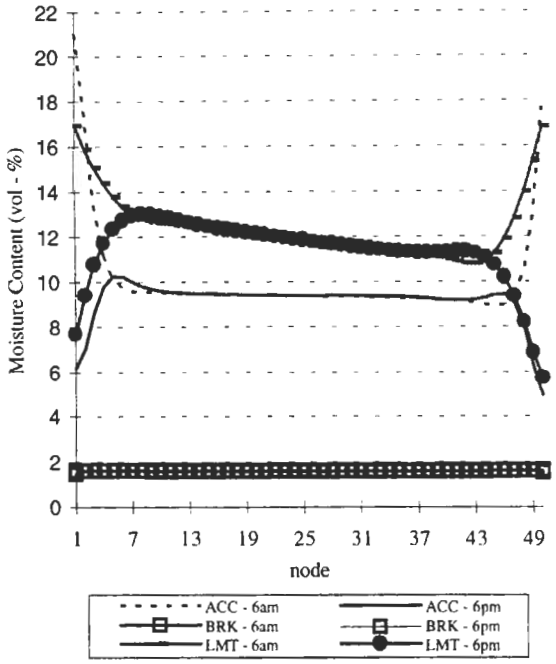

Figure 2: Calculated moisture profiles for "moist" simulation of 10-cm thick autoclaved cellular concrete (ACC), brick (BRK) and lime mortar (LMT) walls at 6am and 6pm on February 20 in Florianopolis, Brazil.

"Dry" Vs. "Moist" Simulation

The temperature distributions for "moist" and "dry" cases for ACC are shown in Figure 3. We see at 6pm that the "dry" and "moist" simulation curves have similar behavior; however, at 6am, when the moisture content is high (see Figure 2), there is a large temperature difference on the inside surface between the "moist" and "dry" simulations. Most noticeable is a 2.0°F (1.1 °C) difference between the "moist" and "dry" simulations for the ACC wall at 6am.

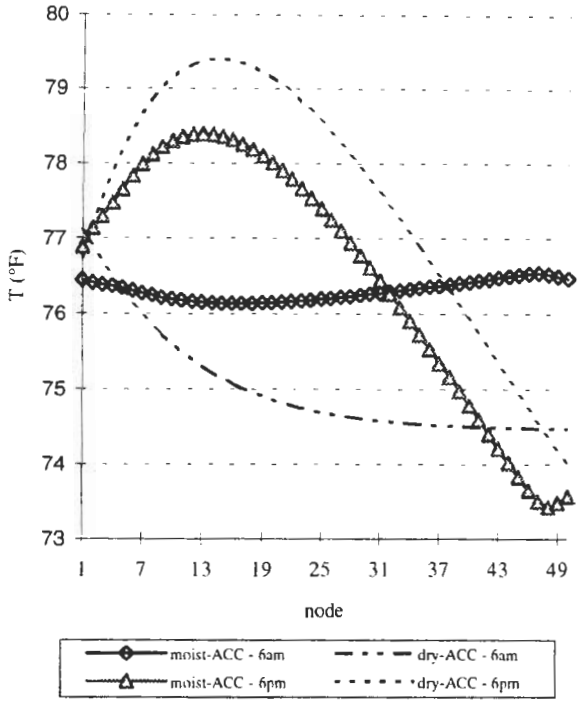

Figure 3: Calculated temperature profiles for "moist" and "dry" simulation of autoclaved cellular concrete (ACC) at 6am and 6pm on February 20.

Sunny Day Comparison

Figure 4 compares the sensible, latent and total heat fluxes on February 21 for "moist-sunny" and "dry-sunny" simulations of an AAC wall. When the air conditioner is turned on in the early morning the latent heat flux rises substantially due the low relative humidity of the room air imposed by the machine. It takes about 3 hours to reach a stable room air condition at 11 am. In this period we see the greatest difference between the simulation with and without moisture migration since the air conditioner dries the air to 60% RH. At 5 pm, when the machine is turned off, the indoor air loses moisture to the wall.

The basic differences between the "moist" and the "dry" simulations are due to a combination of phase change effects, which are present for the "moist" but not the "dry" simulation, and the higher thermal mass and thermal conductivity for the "moist" simulation. At night, when the outside temperature decreases, the higher thermal mass delays the temperature decrease on the inside wall surface; however, the higher thermal conductivity and the phase change cause the inside surface temperature to decrease rapidly, which makes the "moist-sunny" sensible load less than the "dry-sunny" sensible load in this case. If this had not happened the difference between the the "moist-sunny" and "dry-sunny" total load would be even greater. Curves similar to those in Figure 4 are observed for the other materials (not shown).

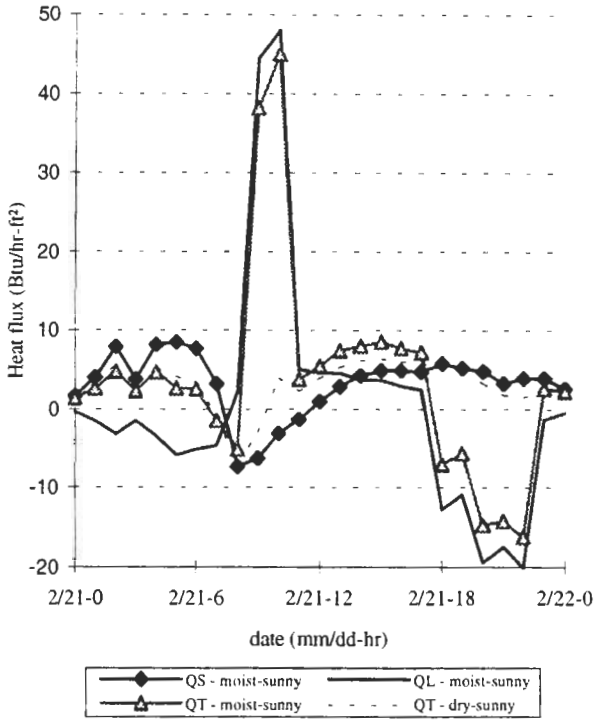

Figure 4: Inside surface sensible (QS), latent (QL) and total (QT) heat fluxes for an autoclaved cellular concrete wall on February 21 for "moist-sunny" and "dry-sunny" simulations.

Cloudy Day Comparison

Figure 5 compares the cooling loads on a cloudy day for a brick wall for "rainy-cloudy", "moist-cloudy" and "dry-cloudy" simulations. The absence of solar radiation increases the influence of moisture on the cooling load since, in this case, there is less evaporation from the outside surface and, therefore, the wall stays moister. Of course, the wetter the wall the greater is the difference expected between the "moist" and "dry" simulations. (This is also observed below in the energy use analysis shown in Figures 6 and 7.)

Figure 5 shows that after 1pm the ratio between the "rainy-cloudy" load (with θ_{mean}=12.5% at 3pm) and the "moist-cloudy" load (with θ_{mean} = 1.6% at 3pm) is almost constant (about 1.5).

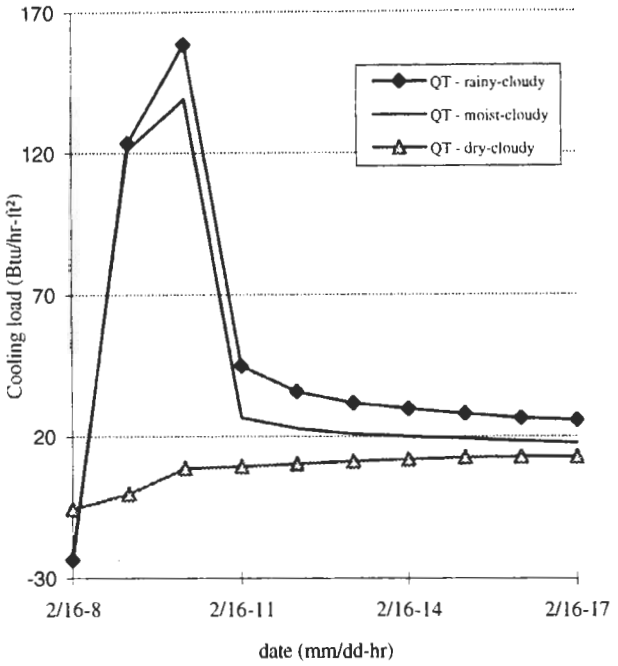

Figure 5: Comparison between conduction cooling loads on a cloudy day for a brick wall for "rainy", "moist" and "dry" simulations.

Since intermittent air conditioning is not taken into account, the difference between the "dry" and the "moist" or "rainy" simulations tends to decrease, because the latent heat transfer to the indoor air decreases.

Daily Cooling Load and Influence of Rain and Solar Radiation

Next, we show, in Figures 6 and 7, the daily cooling load for sunny and cloudy weeks.

We see that the brick wall has the highest cooling load, except in the "dry" simulation, for which lime mortar has the highest cooling load; this illustrates the effects of moisture migration.

We note that the "rainy" simulation doesn't always show the highest cooling load. This is due to the appearance of a negative moisture gradient, or because the sensible load decreases due to a decrease in temperature gradient. For the "rainy" simulation we have assumed a mean moisture content of 20% at the beginning of the week, which leads to a higher latent load.

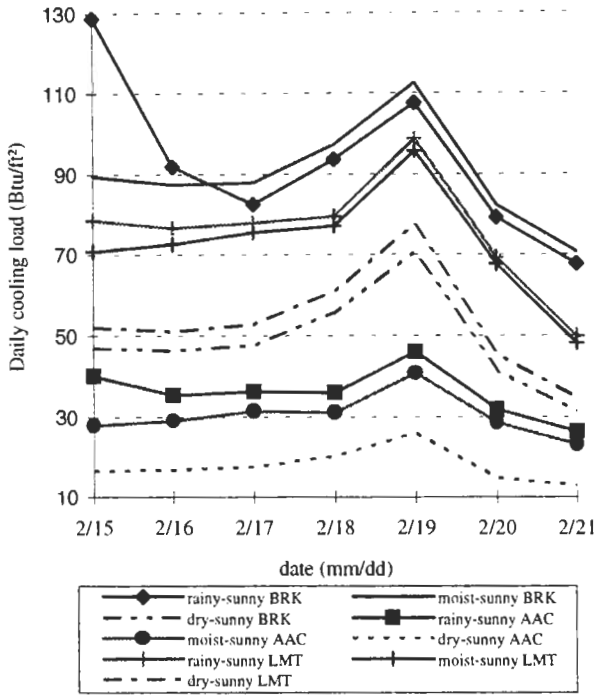

Figure 6: Daily cooling load associated with wall conduction for brick (BRK), lime mortar (LMT) and autoclaved cellular concrete (ACC) for a sunny week for "rainy", "moist" and "dry" simulations.

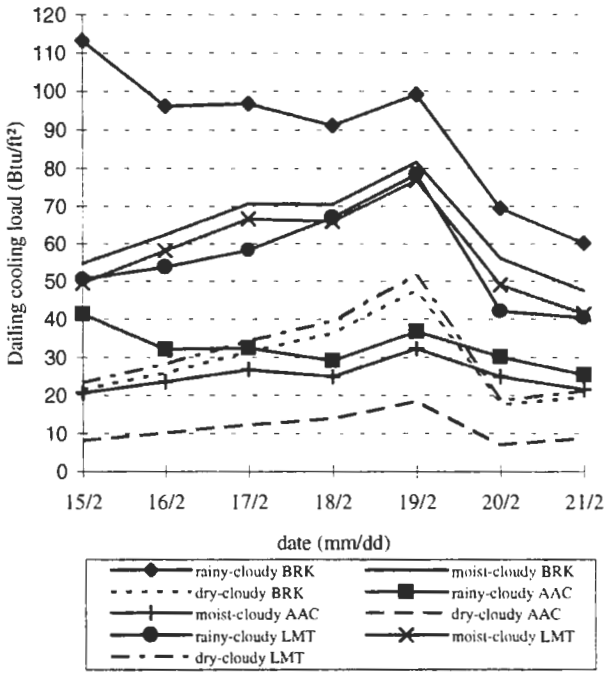

Figure 7. Daily cooling load associated with wall conduction for brick (BRK), lime mortar (LMT) and autoclaved cellular concrete (ACC) for a cloudy week for "rainy", "moist" and "dry" simulations.

The effect of solar radiation and moisture content on coupled heat and mass transfer through porous materials is given in Figure 8, which shows the cooling loads (sensible plus latent) for an ACC wall for sunny and cloudy conditions. We see that solar radiation has a minor influence: even though solar radiation produces higher outside surface temperatures, the cooling loads are lower than those for cloudy conditions. This is primarily due to latent heat effects on the inside surface.

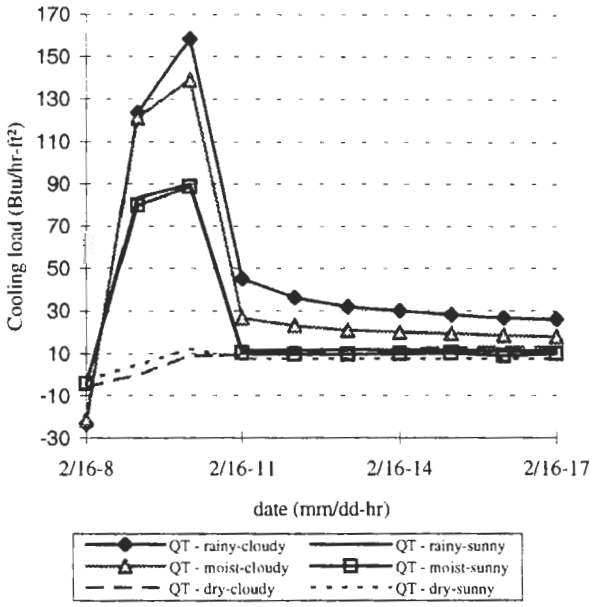

Figure 8: Comparison among cooling loads for cloudy and sunny conditions for an autoclaved cellular concrete wall on February 16, for "rainy", "moist" and "dry" simulations.

The data used in Figures 6 and 7 are given in Tables 2 and 4, respectively, of the Appendix. From these tables we observe that the difference between "dry" simulation and "moist" or "rainy" simulation is largest for brick walls. Tables 3 and 5 of the Appendix give the relative errors in cooling energy use in "dry" vs. "moist" or "rainy" simulation. Lime mortar walls have the lowest error.

5. CONCLUSIONS

The model presented here allows calculation of sensible and latent heat transfer through walls. Higher accuracy in the heat tranfer calculation and the associated cooling load calculation is achieved by allowing the basic thermal properties of the wall material to depend on moisture content. It was shown that large errors in sensible and latent heat transfer can result if moisture migration and the dependence of thermal properties on moisture content are neglected. The errors are largest in the morning when the cooling system turns on and a large latent load due to moisture extracted from the walls can occur. As shown in Figures 4, 5 and 8, significant errors can also occur in the afternoon when the latent heat effect is smaller.

From Appendix Tables 3 and 5 for sunny week "moist" simulations we saw a minimum mean error of 27% for a lime mortar and a maximum error of 46% for brick. These errors are higher for the cloudy week since the moisture content is higher, with a minimum mean error of 48% for lime mortar and a maximum error of 56% for brick.

The effects of extremely high moisture content were illustrated by simulating rain-soaked materials with no moisture barrier.

It was shown quantitatively how walls in a hot/humid climate dry out and produce a latent cooling load when the air conditioning system is turned on, and how wall moisture builds up again when the system turns off.

In conclusion, we have shown the importance of incorporating combined heat and mass transfer into building energy simulation software to more accurately calculate cooling loads in hot and humid climates.

6. NOMENCLATURE

c	specific heat [Btu/lbm-°F].
DBT	dry bulb temperature [°F].
D_{Tl}	liquid phase transport coefficient associated with a temperature gradient [ft^2/s-°F].
D_{Tv}	vapor phase transport coefficient associated with a temperature gradient [ft^2/s-°F].
$D_{\theta l}$	liquid phase transport coefficient associated with a moisture content gradient [ft^2/s].
$D_{\theta v}$	vapor phase transport coefficient associated with a moisture content gradient [ft^2/s].
D_T	mass transport coefficient associated with a temperature gradient [ft^2/s-°F].
D_θ	mass transport coefficient associated with a moisture content gradient [ft^2/s].
h	heat convection transfer coefficient [Btu/hr-ft^2-°F].
h_m	mass convection transfer coefficient [ft/s].
j_l	liquid flux [lbm/ft^2-s].

j_v	vapor flux [lbm/ft^2-s].
l	wall thickness [ft].
L	heat of vaporization [Btu/lbm].
qr	short wave solar radiation [Btu/hr-ft^2].
QL	latent heat flux [Btu/hr-ft^2].
QS	sensible heat flux [Btu/hr-ft^2].
QT	total heat flux [Btu/hr-ft^2].
RH	relative humidity.
T	temperature [°F].
t	time [s].
x	distance into wall [ft].
α	solar thermal radiation absorptance.
η	porosity.
λ	thermal conductivity [Btu/hr-ft-°F].
θ	moisture volumetric content [ft^3 of water / ft^3 of porous material].
ρ	mass density [lbm/ft^3].

Subscripts

ext	exterior air.
int	interior air.
l	liquid.
m	mean.
o	solid matrix.
s	solid.
v	vapor.

7. ACKNOWLEDGMENTS

The authors thank CNPq - Conselho Nacional de Desenvolvimento Científico e Tecnológico of the Secretary for Science and Technology of Brazil, UFSC, Federal University of Santa Catarina, Florianópolis, Brazil for support of this work. One of the authors (Nathan Mendes) gives special thanks to Lawrence Berkeley National Laboratory for its technical support and hospitality.

8. REFERENCES

1. Bogle A., McMullan J.T. and Morgan R., "An Experimental Examination of the Effects of Rainfall on the Heat Loss from a Red Brick Wall", Energy Research, Vol. 8, 1-18, 1984.

2. Burch D.M. and Thomas W.C., "An Analysis of Moisture Accumulation in Wood Frame Wall Subjected to Winter Climate", NISTIR 4674, Gaithersburg, MD: National Institute of Standards and Technology, 1991.

3. Cunningham M.J., "The Moisture Performance of Framed Structures: A Mathematical Model", Bldg Envir. 23, pp 123 - 135, 1988.

4. Da Cunha Neto, J. A. B., "Transport d'humidité em matériau poreux en présence d'un gradient de température. Caractérisation expérimentale d'un béton cellulaire", Thèse de Docteur, Grenoble, Université Joseph Fourier, Grenoble, 1992, 194p.

5. El Diasty R., Fazio P. and Budaiwi I., "Dynamic Modelling of Moisture Absorption and Desorption in Buildings", Bldg Envir. 28, pp 21-32, 1993.

6. Keresteciogiu A. and Gu L., "Incorporation of the Effective Penetration Depth Theory into TRNSYS", Draft Report, Florida Solar Energy Center, Cape Canaveral, Florida, 1989.

7. Liesen, R.J., "Development of a Response Factor Approach for Modeling the Energy Effects of Combined Heat and Mass Transfer with Vapor Adsorption in Building Elements", Ph.D. thesis, Mechanical Engineering Department, University of Illinois, 1994.

8. Patankar S.V., Numerical Heat Transfer and Fluid Flow, McGraw-Hill, 1981.

9. Perrin, B., "Etude des transferts couplés de chaleur et de masse dans des matériaux poreux consolidés non saturés utilisés en génie civil", Thèse Docteur D'Etat, Toulouse, Universite Paul Sabatier de Toulouse, 1985. 267p.

10. Philip, J. R. and De Vries, D. A., "Moisture movement in porous materials under temperature gradients",Transactions of the American Geophysical Union. v.38, n.2, p.222-232, 1957.

11. Yik F.W.H., Underwood C.P. and Chow W.K., "Simultaneous Modelling of Heat and Moisture Transfer and Air-conditioning Systems in Buildings", Proc. IBPSA Building Simulation '95, 4th International Conference, Madison, WI, USA, 1995.

9. APPENDIX

Table 2: Daily cooling loads (Btu/ft^2) for different materials for a sunny week from 2/15 to 2/21.

	Brick (BRK)			Autoclaved Cellular Concrete (ACC)			Lime Mortar (LMT)		
Date	rainy	moist	dry	rainy	moist	dry	rainy	moist	dry
2/15	128.79	89.63	47.01	40.24	27.92	16.59	78.51	70.95	52.15
2/16	91.89	87.43	46.45	35.47	29.07	16.80	76.71	72.63	51.13
2/17	82.56	87.96	47.76	36.33	31.37	17.53	77.87	75.56	52.85
2/18	93.79	97.42	55.69	35.99	31.09	20.24	79.48	77.08	61.02
2/19	107.84	112.68	70.73	46.08	40.83	26.07	98.90	95.77	77.51
2/20	79.14	82.41	41.44	31.85	28.49	14.80	69.28	67.73	45.48
2/21	67.71	70.73	31.48	26.36	23.16	12.96	49.97	48.15	35.00

Table 3: Percent relative error in daily cooling loads for "dry" vs. "moist" or "rainy" simulations for a sunny week from 2/15 to 2/21.

	"Dry" Vs. "moist" simulations			"Dry" Vs. "rainy" simulations		
Date	BRK	ACC	LMT	BRK	ACC	LMT
2/15	47.55	40.58	26.49	63.50	58.76	33.57
2/16	46.88	42.21	29.60	49.45	52.64	33.35
2/17	45.71	44.12	30.05	42.15	51.76	32.13
2/18	42.83	34.89	20.84	40.62	43.75	23.23
2/19	37.23	36.16	19.06	34.41	43.43	21.62
2/20	49.71	48.04	32.86	47.64	53.53	34.36
2/21	55.50	44.07	27.32	53.51	50.84	29.96
mean	46.49	41.44	26.60	47.33	50.67	29.75

Table 4: Daily cooling loads (Btu/ft^2) for different materials for a cloudy week from 2/15 to 2/21.

	Brick (BRK)			Autoclaved Cellular Concrete (ACC)			Lime Mortar (LMT)		
Date	rainy	moist	dry	rainy	moist	dry	rainy	moist	dry
2/15	113.30	54.77	21.54	41.48	20.68	8.20	50.62	49.58	23.40
2/16	96.30	62.36	25.95	32.08	23.48	10.19	53.82	58.19	28.20
2/17	97.00	70.72	31.40	32.56	26.67	12.29	58.33	66.73	34.30
2/18	91.24	70.52	36.36	29.17	24.93	13.96	67.01	65.99	39.64
2/19	99.34	81.77	47.51	36.91	32.38	18.40	78.43	76.91	51.79
2/20	69.58	56.14	17.66	30.04	24.80	7.07	42.06	49.06	18.68
2/21	60.25	47.57	19.53	25.38	21.47	8.70	40.51	41.50	21.11

Table 5: Percent relative error in daily cooling loads for "dry" vs. "moist" or "rainy" simulations for a cloudy week from 2/15 to 2/21.

	"Dry" Vs. "moist" simulations			"Dry" Vs. "rainy" simulations		
Date	BRK	ACC	LMT	BRK	ACC	LMT
2/15	60.68	60.36	52.81	80.99	80.24	53.78
2/16	58.39	56.60	51.54	73.06	68.23	47.61
2/17	55.61	53.93	48.59	67.63	62.26	41.19
2/18	48.44	44.01	39.93	60.15	52.15	40.84
2/19	41.90	43.17	32.66	52.17	50.15	33.96
2/20	68.55	71.48	61.93	74.62	76.46	55.59
2/21	58.95	59.49	49.12	67.59	65.72	47.89
mean	56.07	55.58	48.08	68.03	65.03	45.84